

Where to Go Next Day: Multi-scale Spatial-Temporal Decoupled Model for Mid-term Human Mobility Prediction

Zongyuan Huang[†], Weipeng Wang[†], Shaoyu Huang, Marta C. González, Yaohui Jin*, *Member, IEEE*, Yanyan Xu*

Abstract—Predicting individual mobility patterns is crucial across various applications. While current methods mainly focus on predicting the next location for personalized services like recommendations, they often fall short in supporting broader applications such as traffic management and epidemic control, which require longer period forecasts of human mobility. This study addresses mid-term mobility prediction, aiming to capture daily travel patterns and forecast trajectories for the upcoming day or week. We propose a novel Multi-scale Spatial-Temporal Decoupled Predictor (MSTDP) designed to efficiently extract spatial and temporal information by decoupling daily trajectories into distinct location-duration chains. Our approach employs a hierarchical encoder to model multi-scale temporal patterns, including daily recurrence and weekly periodicity, and utilizes a transformer-based decoder to globally attend to predicted information in the location or duration chain. Additionally, we introduce a spatial heterogeneous graph learner to capture multi-scale spatial relationships, enhancing semantic-rich representations. Extensive experiments, including statistical physics analysis, are conducted on large-scale mobile phone records in five cities (Boston, Los Angeles, SF Bay Area, Shanghai, and Tokyo), to demonstrate MSTDP’s advantages. Applied to epidemic modeling in Boston, MSTDP significantly outperforms the best-performing baseline, achieving a remarkable 62.8% reduction in MAE for cumulative new cases.

Index Terms—Individual Human Mobility, Mid-term Prediction, Spatial-Temporal Model, Urban Computing, Epidemic Spreading Analysis

I. INTRODUCTION

Human mobility modeling has attracted considerable attention in fields such as commercial planning, healthcare, urban management, and mobile and network applications [1]–[4]. With the rapid advancements in technology, diverse mobility data are now being collected from multiple sources, driving innovation and application across these domains. For example, location-based social network (LBSN) data from check-in services like Yelp and Foursquare enable targeted, location-aware advertising [5]. Mobility trajectories obtained from

Z. Huang, W. Wang, S. Huang, Y. Jin, Y. Xu are with the MoE Key Laboratory of Artificial Intelligence and AI Institute, Shanghai Jiao Tong University, Shanghai 200240, China, and also with the Data-Driven Management Decision Making Lab, Shanghai Jiao Tong University, Shanghai 200240, China. E-mail: {herozen, weipeng001, leak_ish, jinyh, yanyanxu}@sjtu.edu.cn.

M. C. González is with the CEE department, University of California, Berkeley, CA 94720, USA. M. C. González is with the Laboratory DCRP, University of California, Berkeley, CA 94720, USA. M. C. González is with Energy Technologies Area, Lawrence Berkeley National Laboratory, Berkeley, CA 94720, USA. E-mail: martag@berkeley.edu.

[†] Equal contribution.

* Corresponding authors.

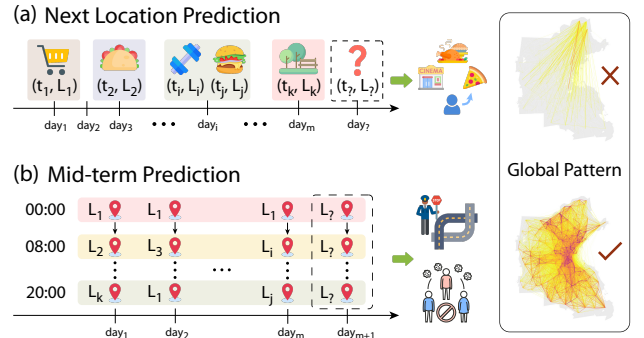


Fig. 1. Task illustrations of next location prediction and mid-term prediction.

mobile devices are instrumental in analyzing and controlling the spread of epidemics [6]–[8], while GPS data from vehicles plays a crucial role in optimizing traffic flow and management [9]–[11]. These developments underscore the growing importance of accurate mobility models in addressing complex real-world challenges.

Human mobility prediction is generally addressed at two scales: collective and individual [12]. This study concentrates on the individual scale, with a specific emphasis on predicting personal mobility patterns. The core challenge in individual mobility prediction revolves around next-location forecasting, which aims to predict an individual’s future destinations based on their historical movement data. Mobility trajectories are commonly represented as sequences of locations, and the primary task is to extract meaningful transition patterns from these sequences. By identifying regularities and trends in an individual’s movement, this approach seeks to enhance the precision of mobility predictions. Traditional models rely on Markov chains [13], while deep learning models apply advanced techniques such as Recurrent Neural Networks (RNNs) and Transformers [14]–[16]. Owing to the spatial characteristics of locations, researchers have explored specific modules to capture spatial relationships. In recent years, the advent of graph representation learning techniques has demonstrated promising potential, motivating the adoption of Graph Neural Networks (GNNs) to enhance the predictive performance [17]–[21].

Next location prediction is widely applied for personalized services, such as recommending points of interest (POI), as illustrated in Figure 1(a). However, urban management applications such as travel management and epidemic transmission

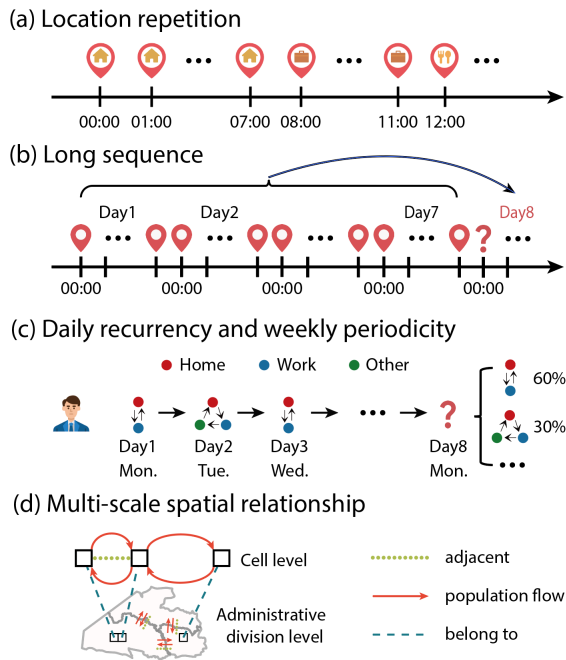


Fig. 2. Characteristics of mid-term mobility prediction.

analysis necessitate predicting residents’ comprehensive trajectory for the next day. This form of prediction, referred to as mid-term prediction, emphasizes modeling complete daily travel behaviors, as depicted in Figure 1(b). To tackle the mid-term prediction task, typical next location prediction models often employ an iterative mechanism to forecast next-day travel behaviors. This involves using predicted outcomes alongside historical data to forecast the remaining trips on the following day. Despite these efforts, these methods present difficulties in achieving satisfactory results, as evidenced in our experiments. Consequently, we propose an effective solution tailored specifically for the mid-term prediction task.

The characteristics of mid-term prediction are illustrated in Figure 2. Firstly, accurate prediction of an individual’s daily trajectory requires knowing their location at each time interval. However, a prolonged stay at a specific location results in consecutive repetitions of the same location within the location sequence. For instance, hourly observations often show repeated instances of home occupancy during the nighttime and early morning, as illustrated in Figure 2(a). Such consecutive location repetitions in trajectory sequences confound the sequence models in accurately identifying location transitions. Secondly, learning the daily travel patterns over multiple days is essential for accurately predicting future behaviors. Yet, the long location sequences pose challenges to the perception and memory capabilities of sequence models, as indicated in Figure 2(b). Thirdly, people’s daily travel activities exhibit multi-scale regular patterns such as daily recurrency and weekly periodicity. Daily recurrency describes the similarity of individual travel behavior day-to-day. Urban residents’ daily travel is typically concentrated in certain primary travel patterns. For instance, as depicted in Figure 2(c), approximately 60% of the individual’s workday trips involve

commuting between home and work, while around 30% involve visiting other places after work before returning home. On the other hand, weekly periodicity signifies the cyclical travel patterns, for instance, similarities in travel behaviors between Mondays. These patterns are essential for the modeling of daily trajectories. Lastly, cities display diverse spatial relationships among their regions, encompassing proximity, population flows, and significant administrative connections, as exemplified in Figure 2(d). Multiscale spatial granularity provides diverse insights into urban structural features, aligning with the multiscale characteristics encompassing both short and long-distance travel. Investigating these multiscale spatial relationships can enhance location representations and improve model performance in downstream tasks.

In this paper, we propose a Multi-Scale Spatial-Temporal Decoupled Predictor (MSTDP) for the mid-term prediction task. Our approach starts by decoupling individuals’ daily trips into separate location and duration chains, thereby eliminating consecutive repetitions and directly capturing the daily transition patterns. Following this, a two-layer hierarchical encoder is employed to extract multi-scale temporal patterns like daily recurrency and weekly periodicity, efficiently broadening the receptive field and capturing longer-term behavioral regularities. Subsequently, a Transformer-based decoder integrates encoded historical information and previously predicted partial results to forecast trajectories for the following day. Furthermore, we introduce a heterogeneous graph module to capture the spatial and accessibility relationships between regions at different scales, thereby enriching the semantic representation of locations and enhancing predictive accuracy. We evaluate MSTDP against nine baselines using five urban-scale mobile record datasets. Empirical results demonstrate the superior performance of the proposed model. We further conduct comprehensive statistical physics analyses using Boston as a case study, examining motifs, travel distances, origin-destination flows, and other dimensions to provide a multidimensional assessment of the model’s effectiveness. Moreover, we utilize the model’s predictions to analyze the epidemic transmission dynamics. Specifically, we simulate the epidemic spread using the SEIR model [22] and the population transfer probability matrices derived from travel trajectories. This enables monitoring of the cumulative new cases and the current active cases. Compared to the baseline, MSTDP demonstrated remarkable improvements with reductions in MAE by 87.6% for the cumulative new cases and 62.8% for the current active cases, highlighting the superior predictive capability of our model in modeling travel behaviors.

We summarize the key contributions as follows:

- We highlight mid-term mobility prediction, a crucial task distinct from next-location prediction. This task concentrates on the daily mobility patterns of urban populations, supporting applications in urban management such as disease control and traffic regulation.
- We propose a novel Multi-scale Spatial-Temporal Decoupled Predictor (MSTDP), employing a spatial-temporal decoupling approach to address repeated observations and hierarchical encoders to efficiently capture the multi-scale temporal patterns, including daily recurrence and weekly

periodicity of travel behavior.

- We introduce a novel spatial heterogeneous graph to describe the multi-scale location relationships, including mobility flow and adjacent relationships across regions at different scales. To capture these relationships, we develop a graph network-based heterogeneous geospatial module, enhancing the semantic richness of location representations.
- Extensive experiments on five urban datasets validate the effectiveness of the proposed model. We provide diverse statistical physics analysis perspectives for comprehensive evaluation. Moreover, we apply the model's predictions to analyze the epidemic transmission in Boston, demonstrating the significant advantages of MSTDP.

II. RELATED WORK

Human mobility modeling typically employs sequential models to capture the transition relationships between locations. Early methods mainly rely on Markov Chain to construct location transition probability matrices, with techniques to incorporate temporal and spatial information to capture individual travel preferences [13], [23], [24]. The evolution of deep learning has effectively facilitated the modeling of complex interactions. The foundational framework of location sequence models has progressed from the RNN series [14], [25], [26] to attention-based Transformer architectures [15], [16], consequently enhancing the capacity to capture high-order transition patterns. In addition to the transition regularity, location sequences offer a wealth of spatiotemporal information. Thus, researchers have introduced innovative mechanisms from diverse perspectives such as temporal and spatial semantics to enhance sequence models [27]–[34]. Besides, some work also incorporates location category information to further constrain the location selection [35]–[37]. However, these methods would encounter several challenges when applied to the mid-term mobility prediction task, as discussed in Introduction I. At present, there is limited research dedicated to mid-term behavioral prediction tasks, such as HTAED [38] and RLMob [39]. But both models still face difficulties including repeated consecutive locations and excessively long sequences, and they inadequately capture the multi-scale spatiotemporal patterns inherent in individual daily travel. To mitigate their limitations, we propose a spatiotemporal decoupled hierarchical framework, including a heterogeneous graph learner, which enlarges the perception field and efficiently captures the multi-scale spatiotemporal periodic information.

Over the past few years, graph neural networks have enjoyed rapid development and have been increasingly applied to learn location representations [18], [40]–[43]. Researchers customarily construct a flow graph and an adjacency graph, from which they derive two distinct location representations and devise mechanisms to effectively combine them [17], [19], [44]. In this work, we integrated these two graphs into a heterogeneous graph to learn an informative location representation. Additionally, our graph considers multi-level adjacency relationships and flow relationships to efficiently capture complex geographic spatial information.

III. PRELIMINARY

In this section, we first formulate the next day mobility prediction task, and then introduce the definition of two basic location graphs.

A. Individual Trajectory

Analyzing individual mobility patterns throughout the day necessitates dense data. To this end, we leverage Call Detail Record (CDR) data, which records locations using latitude and longitude coordinates rather than Points of Interest (POI) as in LBSN data. To address privacy concerns and simplify the modeling process, researchers partition the urban area into grid cells of equal size and map individuals' trajectories to cells. Each grid cell is treated as a discrete location visited by individuals [24]. The cell size used in this study is $1 \text{ km} \times 1 \text{ km}$. Here, the location set is denoted as $\mathcal{L} = \{l_1, \dots, l_{|\mathcal{L}|}\}$. We then partition each day into fixed-size timeslots. Using an hourly time window as an example, the daily trajectory is expressed as $D = \{l_p^0, \dots, l_q^{23}\}$, where l_p^t denotes the stay location l_p within the hour $[t, t + 1)$, $t \in \mathbb{N}$. Let $U = \{u_1, \dots, u_{|U|}\}$ denotes a set of individuals. Then all of trajectories of an individual u can be represented as $\text{TRAJ}_u = \{D_1, \dots, D_N\}$, where N is the number of total trajectories of the user, $N = |\text{TRAJ}_u|$.

Task Formulation. Given an individual u and his or her historical trajectories $\{D_1, \dots, D_k\}$, the goal is to predict the next day trajectory $\hat{D}_{k+1} = \{\hat{l}_p^0, \dots, \hat{l}_q^w\}$, where $k \leq |\text{TRAJ}_u| - 1$. w is determined by the size of the time window. In the methodology section, we present the model's details using hour-long windows as an example. In the experiments, different datasets require varying time window sizes, selected based on the level of data sparsity.

B. Basic Location Graph

The flow graph and adjacency graph have been used in recent studies to capture the spatial relationships of locations [17]–[19]. We define these two graphs as follows.

Flow Graph is a directed graph $G^f = (V, E^f)$ to describe transition relationships among locations, where the node $v_j, v_j \in V$, denotes a location, the edge $e_{pq}^f, e_{pq}^f \in E^f$, represents the number of trips from v_p to v_q produced by all individuals. In this study, we only count E^f in the training set.

Adjacency Graph is an undirected graph $G^a = (V, E^a)$ to depict the proximity between locations. The node set V aligns with the location set in the flow graph G^f . The undirected edge e_{pq}^a in the edge set E^a indicates that the geospatial distance between v_p and v_q , denoted as dist_{pq} , is less than a pre-defined threshold \bar{d} . In our work, \bar{d} is set to 2 km for a cell with 1 km width. $e_{pq}^a = 1$ if $\text{dist}_{pq} \leq \bar{d}$ and $e_{pq}^a = 0$ otherwise.

IV. METHODOLOGY

In this section, we will sequentially introduce the four primary components of the Multi-scale Spatial-Temporal Decoupled Predictor (MSTDP), as illustrated in Figure 3.

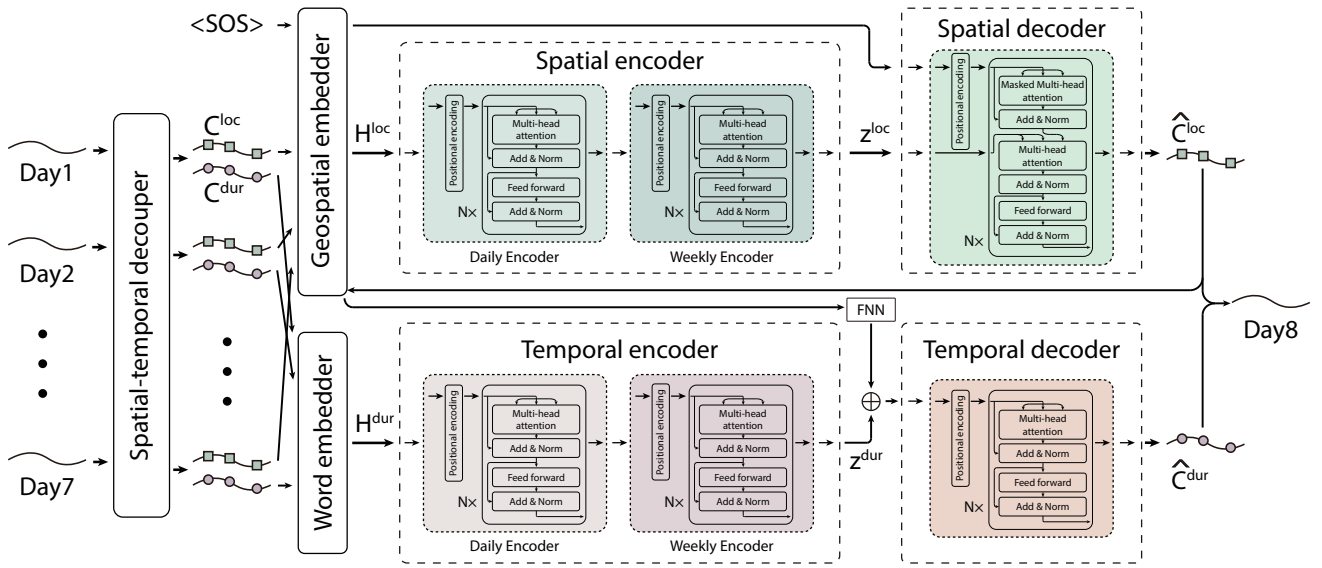


Fig. 3. The framework of the proposed Multi-scale Spatial-Temporal Decoupled Predictor (MSTDP).

A. Spatial-Temporal Decoupler

Modeling the daily travel behavior of individuals at the urban scale presents challenges of location repetition and excessively long sequences, as mentioned in Introduction I. Location repetition arises from individuals being observed multiple times at the same location due to their prolonged stays. Therefore, we can extract the stay duration from a daily trajectory to obtain the location sequence that eliminates consecutive repetitions. Specifically, the proposed spatiotemporal decoupler separates the trajectory of the k -th day D_k into a location chain $C_k^{\text{loc}} = \{l_p, \dots, l_q\}$ and a duration chain $C_k^{\text{dur}} = \{t_1, \dots, t_n\}$, where $t \in \mathbb{N}^+$ and $\sum_{s=1}^n t_s = 24$. The elements t_i in the duration chain correspond to the stay duration in the i -th location of C_k^{loc} . Both chains are of equal lengths $|C_k^{\text{loc}}| = |C_k^{\text{dur}}|$. Taking a daily trajectory $\{l_1^0, l_1^1, l_2^2, l_3^3, l_4^4, \dots, l_{21}^{21}, l_{22}^{22}, l_{23}^{23}\}$ as an example, the decoupled location and duration chains would be $\{l_1, l_2, \dots, l_3, l_1\}$ and $\{3, 2, \dots, 1, 2\}$ respectively. In this way, we can disentangle lengthy sequences with consecutively repeated locations into two shorter chains, effectively reducing the complexity of pattern learning. Moreover, the decoupled location chain can be viewed as a location-specific motif [45] that enables the model to learn the integrity of an individual's daily travel patterns and the cyclical nature of their everyday behavior.

B. Geospatial Embedder

Locations inherently possess spatial semantic information, inspiring the utilization of graph neural networks to learn location representation from the adjacency graph and flow graph [17], [19], [44]. However, these methods tend to learn embeddings independently from each graph and then merge the embeddings as the location representation, disregarding the interdependencies between the two graphs. Towards this, we introduce a heterogeneous graph, as illustrated in Figure 4, that combines both flow and adjacency relationships between locations. Furthermore, we expect to integrate multi-scale

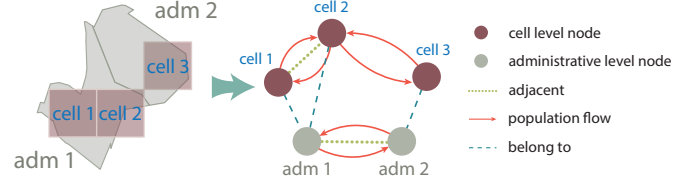


Fig. 4. The illustration of the heterogeneous graph.

urban structural information into the graph. Considering the administrative divisions among regions, we build an administrative level graph with the administrative areas as nodes to enrich the spatial connections between locations. In this way, the heterogeneous graph considers both the cell-level and administrative level flow and adjacency relationships, along with the inclusion relationship between cells and administrative areas. The scale of administrative areas can be chosen as block, tract, town, etc.

We formulate the heterogeneous graph as $G^H = (V_{\text{cell}}, V_{\text{adm}}, E_{\text{cell}}^f, E_{\text{adm}}^f, E_{\text{cell}}^a, E_{\text{adm}}^a, E^i)$, where V_{cell} and V_{adm} are the node sets of cell and administrative area, E_{cell}^f and E_{adm}^f ($* \in [\text{cell}, \text{adm}]$) are the flow and adjacency edge sets, and E^i is the inclusion edge sets. The undirected edge $e_{pq}^i, e_{pq}^i \in E^i$, means that the cell v_p^{cell} is located in the administrative area v_q^{adm} . The description of edges in E_{cell}^f and E_{adm}^f remain consistent with Preliminary III. Moreover, the flow edge in our study includes hourly population flow between connected nodes. The edge is defined as $e_{pq}^f = \{f_{pq}^0, \dots, f_{pq}^{23}\}$, where f_{pq}^t means the number of trips from v_p to v_q during the time interval from the hour t to $(t+1)$, $t \in [0, 23]$.

The node embeddings incorporate neighbor information from various edges to enhance the semantic richness. We employ different message-passing mechanisms based on the characteristics of the heterogeneous edges. Due to the simplistic semantics of the adjacent edge and the inclusion edge, we apply GraphSage [46] as the backbone to model the message

passing of these two types of edges. The graph layer is defined as:

$$\mathbf{x}_p^{(n)} = W^1 \mathbf{x}_p^{(n-1)} + W^2 \text{mean}_{q \in N(j)} \mathbf{x}_q^{(n-1)}, \quad (1)$$

where $\mathbf{x}^{(n)}$ is node embedding in the n -th layer, W^1 and W^2 are learnable parameters, and ‘‘mean’’ is the mean operator to aggregate the neighborhood. The initial node features $\mathbf{x}^{(0)}$ comprises word embeddings of region IDs and the time-varying population count within the region. Regions refer to cells or administrative areas.

Considering the complexity of semantic information in the flow edges, we employ an edge-considered variant of Graph Attention Network (GAT) [47] for effective modeling:

$$\mathbf{x}_p^{(n)} = \alpha_{pp} W_p^{(n-1)} \mathbf{x}_p^{(n-1)} + \sum_{q \in N(p)} \alpha_{pq} W_q^{(n-1)} \mathbf{x}_q^{(n-1)}, \quad (2)$$

where $W_p^{(n-1)}$ and $W_q^{(n-1)}$ are learnable parameters. The attention coefficient α_{pq} is calculated as:

$$\alpha_{pq} = \frac{\exp(\sigma(\mathbf{a}^T [W_p \mathbf{x}_p || W_q \mathbf{x}_q || W_{pq} \mathbf{e}_{pq}^f]))}{\sum_{s \in N(p) \cup \{p\}} \exp(\sigma(\mathbf{a}^T [W_p \mathbf{x}_p || W_s \mathbf{x}_s || W_{ps} \mathbf{e}_{ps}^f]))}, \quad (3)$$

where σ is LeakyReLU and these \mathbf{x} are the abbreviations of $\mathbf{x}^{(n-1)}$. These $W_*, * \in \{p, q, pq, s, ps\}$ are trainable parameters.

After n -layers heterogeneous graph propagation, we obtain the final cell representation as the learned location embedding. These learning processes can be summarized as:

$$\mathbf{H}_k^{\text{loc}} = \text{GraphEmbedder}(\mathbf{C}_k^{\text{loc}}). \quad (4)$$

C. Hierarchical Trajectory Encoder

Urban residents exhibit multi-scale temporal regularities, such as daily and weekly patterns in their travel routines, as mentioned in the Introduction I. To capture these periodicities more effectively, we introduce a hierarchical trajectory encoder with two layers: the daily encoder and the weekly encoder. The daily encoder captures daily travel transitions, while the weekly encoder focuses on weekly travel variation patterns. By considering information from the corresponding day a week ago and the within-week behavioral changes, our model is capable of predicting trips on the eighth day with enhanced accuracy.

Both the daily encoder and the weekly encoder utilize a positional encoding module and a Transformer encoder [48], denoted as DailyEnc and WeeklyEnc, to capture sequential relationships. The Transformer encoder mainly consists of a multi-head self-attention mechanism and a fully connected feed-forward neural network (FNN). The attention mechanism applies various heads to simultaneously attend to different aspects, enhancing the model to capture complex dependencies from sequences and acquire information-rich representation. The detailed descriptions of the positional encoding module and the attention mechanism refer to [48].

We utilize two hierarchical encoders, namely spatial encoder and temporal encoder, to model the decoupled location chain and duration chain. With the daily encoder, we have the k -th daily chain representation $\mathbf{h}_k^{\text{loc}} \in \mathbb{R}^{d_{hl}}$ and $\mathbf{h}_k^{\text{dur}} \in \mathbb{R}^{d_{ht}}$ as follows:

$$\mathbf{h}_k^{\text{dur}} = \text{DailyEnc}^{\text{dur}}(\mathbf{H}_k^{\text{dur}}), \quad (5)$$

$$\mathbf{h}_k^{\text{loc}} = \text{DailyEnc}^{\text{loc}}(\mathbf{H}_k^{\text{loc}}). \quad (6)$$

d_{hl} and d_{ht} denotes the dimension of $\mathbf{h}_k^{\text{loc}}$ and $\mathbf{h}_k^{\text{dur}}$. $\mathbf{H}_k^{\text{loc}} \in \mathbb{R}^{|\mathbf{C}_k^{\text{loc}}| \times d_{el}}$ is the embedding of location chain $\mathbf{C}_k^{\text{loc}}$ learned with the geospatial embedder, as introduced in the subsection IV-B. $\mathbf{H}_k^{\text{dur}} \in \mathbb{R}^{|\mathbf{C}_k^{\text{dur}}| \times d_{et}}$ is the embedding of duration chain $\mathbf{C}_k^{\text{dur}}$ learned with a word embedder. The word embedder receives the vocabulary size and embedding dimension as input, learning dense vector representations for each word. In contrast to one-hot encoding, it generates more compact and semantically informative embeddings, capturing contextual relationships between words. d_{el} and d_{et} denote the embedding dimension of location and duration. Then we obtain the historical information representation $\mathbf{z}^{\text{loc}} \in \mathbb{R}^{d_{zl}}$ and $\mathbf{z}^{\text{dur}} \in \mathbb{R}^{d_{zt}}$ through the weekly encoder, formulated as:

$$\mathbf{z}^{\text{dur}} = \text{WeeklyEnc}^{\text{dur}}(\{\mathbf{h}_{k-6}^{\text{dur}} \oplus \mathbf{h}_{k-6}^{\text{loc}}, \dots, \mathbf{h}_k^{\text{dur}} \oplus \mathbf{h}_k^{\text{loc}}\}), \quad (7)$$

$$\mathbf{z}^{\text{loc}} = \text{WeeklyEnc}^{\text{loc}}(\{\mathbf{h}_{k-6}^{\text{loc}}, \dots, \mathbf{h}_k^{\text{loc}}\}). \quad (8)$$

d_{zl} and d_{zt} denotes the dimension of \mathbf{z}^{loc} and \mathbf{z}^{dur} . Here, the symbol \oplus represents vector concatenation and the concatenated vector, $\mathbf{h}_k^{\text{dur}} \oplus \mathbf{h}_k^{\text{loc}}$, has the dimension $d^{\text{loc}} + d^{\text{dur}}$. The missing days during a week are masked in the weekly encoder to preserve the temporal structure integrity.

D. Trajectory Decoder

The trajectory decoder is comprised of a spatial decoder and a temporal decoder. Considering the dependency between duration and location, we expect to predict the location chain first and then utilize it to enhance the prediction of the duration chain. Inspired by the natural language process tasks, we add the start and end tokens into the location chain to address the challenges of the unknown start location and the uncertain chain length. Besides, we employ the Transformer decoder [48] as the backbone of the spatial decoder, along with a positional encoding module and an FNN. The self-attention mechanism in the Transformer decoder and positional encodings enable the model to effectively capture long-range dependencies and maintain the temporal order of the input sequence, thereby alleviating accumulative errors in multi-step prediction tasks. Commencing from the start token $\langle \text{SOS} \rangle$, the spatial decoder utilizes the historical information and predicted results to make iterative predictions for the daily location chain. This process is formulated as:

$$\hat{l}_{i+1} = \text{SpatialDec}(\{s_0, \hat{s}_1, \dots, \hat{s}_i\}, z^{\text{loc}}), \quad (9)$$

where SpatialEnc is the abbreviation of the spatial decoder, \hat{s}_i is the embedding of i -th predicted location $\hat{s}_i = \text{GraphEmbed}(\hat{l}_i)$ and s_0 is the embedding of the start token. The iterative prediction process halts upon the prediction of the end token. Consequently, the predicted location chain is $\hat{\mathbf{C}}^{\text{loc}} = \{\hat{l}_1, \dots, \hat{l}_m\}$, with m representing the number of location appeared on the target day.

The temporal decoder comprises a positional encoding module, Transformer encoder, and FNN. We utilize the Transformer encoder to enable the model to employ attention mechanisms for observing daily location access patterns when predicting duration. Historical time data and predicted location

representations are combined into the time encoder to derive the forecasted duration chain, formulated as:

$$\hat{C}^{\text{dur}} = \{\hat{t}_1, \dots, \hat{t}_m\} = \text{TemporalDec}(\{\hat{s}'_1 \oplus z^{\text{dur}}, \dots, \hat{s}'_m \oplus z^{\text{dur}}\}), \quad (10)$$

where `TemporalDec` is the abbreviation of the temporal decoder and \oplus represents vector concatenation as mentioned before. $\hat{s}'_k = \text{FNN}(\hat{s}_k)$, where a FNN is used to adjust the dimension of the predicted location embeddings. Finally, we combine the predicted duration chain and location chain to derive the predicted trajectory for the following day.

E. Model Optimization

We apply the most commonly used cross-entropy loss for the location chain prediction. The Huber loss is used for the duration chain prediction as it integrates the advantages of MSE and MAE. The total loss function is defined as:

$$L = L_{ce}(l_j, \hat{l}_j) + \lambda \cdot L_{huber}(t_j, \hat{t}_j), \quad (11)$$

where $L_{huber}(t_j, \hat{t}_j) = \begin{cases} (t_j - \hat{t}_j)^2, & |t_j - \hat{t}_j| < 1 \\ |t_j - \hat{t}_j| - 1/2, & \text{otherwise} \end{cases}$, $L_{ce}(l_j, \hat{l}_j) = -l_j \log \hat{l}_j$, and λ is a hyperparameter to adjust loss weight. l_j and t_j are the targets, while \hat{l}_j and \hat{t}_j are the predicted values.

V. EXPERIMENTS

A. Experimental Settings

1) *Data Description*: Experiments are conducted on four private¹ urban-scale datasets, *Boston*, *Los Angeles*(LA), *San Francisco Bay Area*(SFBay), *Shanghai*, collected from real-world mobile records, and one public dataset *Tokyo* [49], comprising synthetic mobility data. The preprocessing steps for the CDR datasets follow [24]. Besides, we partition each city into uniform grids with grid sizes of 1 kilometer. As described in Preliminary, a day is divided into multiple time windows, and only the record with the longest stay duration is retained within each window. Boston, LA, and SFBay utilize half-hour windows, whereas Shanghai and Tokyo use hour-long windows. The statistics of the datasets are presented in Table I, where “# Days” means the average number of days and “# Admins” means the number of the administrative division. Boston, LA, and SFBay employ census tracts as administrative units, whereas Shanghai uses towns. In the Tokyo dataset, due to blurred exact coordinates, we partitioned administrative regions using 7x7 grid squares. The training, validation, and test sets are obtained by partitioning the original dataset in a ratio of 6:1:3 based on the time span.

2) *Baselines*: Seven models for predicting next locations and two models for successive mobility prediction are utilized for comparative analysis. They are CFPRec [15], GETNext [16], GFlash [50], HGARN [51], SNPM [41], AGRAN [42], MTNet [33], HTAED [38], and RLMob [39]. A concise introduction to these baselines is listed as follows:

¹The dataset is not publicly disclosed due to privacy constraints.

TABLE I
STATISTICS OF THE PREPROCESSED URBAN-SCALE DATASETS.

Datasets	# Individuals	# Locations	# Admins	# Days	# Records
<i>Boston</i>	50,000	10,294	1,126	39	6,749,540
<i>LA</i>	50,000	6,188	2,493	41	7,768,373
<i>SFBay</i>	50,000	8,032	1,406	41	7,700,986
<i>Shanghai</i>	20,000	16,050	234	99	8,209,910
<i>Tokyo</i>	16,151	7,153	225	75	7,502,839

- **CFPRec** [15] develops a two-layer attention mechanism where future time embeddings are used to query the most valuable historical information.
- **GETNext** [16] utilizes a flow map to learn location representation and a Transformer to encode historical sequences and make predictions.
- **GFlash** [50], originally named Graph-Flashback, designs a knowledge graph to learn the transition probabilities between locations and employs GNNs to learn location representations in a homogeneous graph.
- **HGARN** [51] introduces a hierarchical graph to extract dependencies among activities and locations. The location representations are learned with graph attention networks.
- **SNPM** [41] applies a dynamic graph method to discover neighbors of current locations and learn the location representation, along with an attention-based structure to make predictions.
- **AGRAN** [42] proposes an adaptive graph learning module to learn an optimized topology of location. An attention-based network is adopted to predict locations.
- **MTNet** [33] construct a tree structure from individual trajectories to capture the preferences in multi-granularity time slots.
- **HTAED** [38] introduces an LSTM-based encoder-decoder model with a hierarchical temporal attention module for successive mobility prediction.
- **RLMob** [39] models the successive mobility prediction as Markov Decision Process and proposes an actor-critic framework with an instance of Proximal Policy Optimization (PPO).

3) *Evaluation Metrics*: We evaluate these models with four metrics: *Acc*, *DevDist*, *TravelDist*, and *DepartTime*. *Acc* indicates the proportion of the accurately predicted locations. *DevDist* is the average deviation distance, measured in kilometers, between all actual and predicted locations. *TravelDist* and *DepartTime* quantify the Jensen-Shannon divergence (JSD) between actual and predicted travel distances and departure times for individuals.

Acc and *DevDist* are assessed point-wise, while *TravelDist* and *DepartTime* are evaluated individually. Specifically, *Acc* describes the proportion of the accurately predicted locations, calculated with $Acc = \frac{Count(\hat{l}=l)}{N_l}$, where $Count()$ measures the number of correctly predicted locations, with N_l denoting the total number of locations in the trajectory. *DevDist* measures the averaged deviation distance between actual and predicted locations, formulated with $DevDist = mean_{N_l}(\left(distance(\hat{l}, l) \right))$. $distance()$ calculates the distance between two locations in kilometers, whereas $mean_{N_l}()$

computes the average over N_l locations. *TravelDist* initially computes the distribution of individual travel distances, evaluates the Jensen-Shannon divergence (JSD) between the actual and predicted distributions per individual, and subsequently averages these differences across all users. It is formally defined by $mean_{N_l}(JSD(\hat{p}_{dist}, p_{dist}))$, where \hat{p}_{dist} and p_{dist} denote the predicted and actual distribution of travel distances. The calculation of *DepartTime* is similar to *TravelDist*, focusing on the distribution of departure times. Its formal definition is $mean_{N_l}(JSD(\hat{p}_{time}, p_{time}))$, where \hat{p}_{time} and p_{time} denote the predicted and actual distribution of departure time.

The improved performance is reflected in larger *Acc*, as well as smaller *DevDist*, *TravelDist*, and *DepartTime*.

4) *Implementation*: These baselines are implemented with their open-source codes. Hyperparameter tuning is performed on the validation set to attain optimal performance. The implementation of MSTDP is based on the PyTorch framework. The heterogeneous GNNs adopt a two-layer structure, while the layer numbers of Transformer encoder and decoder are also set to 2. The embedding dimensions of location and time are 512 and 512. The hidden dimensions of location and time are 1024 and 512. The head numbers of attention in the Transformer encoder and decoder are set to 8. We apply the Adam optimizer to train MSTDP with a learning rate of 10^{-4} . The hyperparameter λ is set to 1.

5) *Task Settings*: We evaluate models in two tasks: next day prediction and next week prediction. For next day prediction, all models iteratively forecast the location of the next T timeslots by considering historical information and previously predicted results. This means that the prediction of the i -th location \hat{l}_r^i is based on the true historical information $\{D_0, \dots, D_k\}$ and the predicted locations of the preceding $i-1$ points $\{\hat{l}_p^0, \dots, \hat{l}_q^{i-1}\}$, where $i \in [1, T]$. The one-hour time window corresponds to $T=24$, while the half-hour time window corresponds to $T=48$. Similarly, for next week prediction, the next $7 * T$ locations in the following week are also iteratively forecasted. That is, \hat{D}_{k+i} is predicted with $\{D_0, \dots, D_k\}$ and $\{\hat{D}_{k+1}, \dots, \hat{D}_{k+i-1}\}$, where $i \in [2, 7]$.

B. Metric Comparison

We initially evaluate all models using datasets *Boston*, *Shanghai*, and *Tokyo*, and subsequently select the more recent baselines to compare against datasets *LA* and *SFBay*. The results are exhibited in Table II and Table III. From these results, we draw the following observations and analysis: (1) MSTDP demonstrates superior performance on both datasets, validating its effectiveness in mid-term prediction tasks. Compared to the top-performing baseline, MSTDP exhibits improvements of 3.6% in *Acc*, 9.0% in *DevDist*, 20.3% in *TravelDist* and 19.4% in *DepartTime*. A smaller *DevDist* of MSTDP indicates closer proximity between the predicted and the actual locations. Furthermore, lower metrics for *TravelDist* and *DepartTime* demonstrate improved individual consistency between predicted and actual trajectories regarding travel time and distance patterns in our model. (2) Among these baselines, HTAED excels due to its dual-layer attention mechanism

tailored for successive prediction, effectively weighing intra-day and inter-day behavioral patterns. In contrast, RLMob, which employs a reinforcement learning framework for successive prediction, falls short by relying solely on RNNs to model transition relationships, resulting in less favorable performances. These baselines, initially developed for next-location prediction, overlook temporal patterns such as daily and weekly cycles, which complicates their direct application to mid-term forecasting tasks. Moreover, when applied to *Boston*, *LA*, or *SFBay* datasets, these baseline predictions show significant performance degradation compared to *Shanghai* and *Tokyo*, notably highlighted by SNPM. This discrepancy primarily stems from varying time window sizes across datasets; for instance, *Boston* employs a half-hour window, leading to increased location redundancy and longer daily trajectories. These factors present substantial challenges for model performance, as discussed in Introduction I.

C. Statistical Physics Analysis

The metric comparison in Table II does not sufficiently portray the model’s performance. Therefore, we conduct a comprehensive statistical physics analysis on the *Boston* dataset from multiple perspectives to thoroughly examine the performance of these models.

Daily travel distance. Figure 5 presents the statistical distribution of daily travel distances for individuals. These baselines predict a higher number of zero travel distances. It indicates that the models predict a greater occurrence of “full-day stays at the same location, which we refer to as “full-day stays”. Unlike these baselines, MSTDP demonstrates closer alignment between predicted daily travel distances and actual distributions.

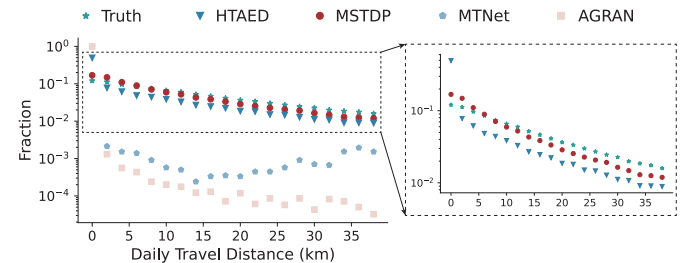


Fig. 5. Daily travel distances.

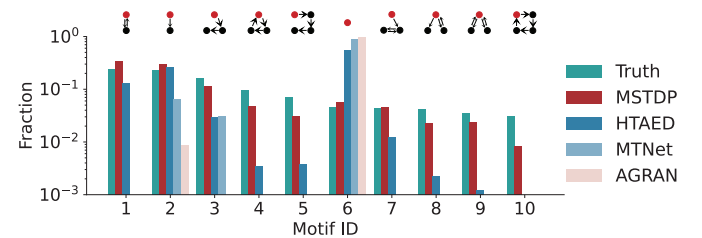


Fig. 6. Top 10 daily motifs.

Human mobility motif. Motif describes people’s mobility pattern during one day with abstract network [45]. Figure 6 illustrates the ten most prevalent motifs in actual daily trajectories, covering 74.6% of the population. MTNet and AGRAN

TABLE II

PERFORMANCE COMPARISON OF ALL METHODS ON THREE REAL-WORLD DATASETS. THE OPTIMAL AND SECOND-BEST RESULTS IN EACH COLUMN ARE HIGHLIGHTED WITH BOLD TEXT AND UNDERLINING.

			CFPRec	GETNext	GFlash	HGARN	SNPM	AGRAN	MTNet	HTAED	RLMob	MSTDP	
Boston	Day	Acc ↑	0.420	0.323	0.360	0.377	0.268	0.496	0.498	<u>0.564</u>	0.363	0.584	
		DevDist ↓	4.991	5.869	6.406	5.855	14.166	5.506	7.969	7.969	<u>4.114</u>	7.744	3.676
		TravelDist ↓	0.655	0.675	0.667	0.621	0.619	0.635	0.650	0.650	<u>0.509</u>	0.606	0.361
		DepartTime ↓	0.541	0.656	0.570	0.656	0.654	0.647	0.658	0.658	<u>0.455</u>	0.636	0.419
	Week	Acc ↑	0.340	0.322	0.351	0.354	0.264	0.371	0.433	0.433	<u>0.444</u>	0.322	0.470
		DevDist ↓	7.470	5.916	6.471	6.603	14.220	6.123	8.357	8.357	<u>5.756</u>	8.236	5.169
		TravelDist ↓	0.652	0.672	0.659	0.627	0.615	0.613	0.671	0.671	<u>0.583</u>	0.681	0.425
		DepartTime ↓	0.571	0.657	0.653	0.604	0.656	0.635	0.669	0.669	<u>0.530</u>	0.668	0.418
Shanghai	Day	Acc ↑	0.557	0.505	0.565	0.569	0.563	0.582	0.540	<u>0.602</u>	0.585	0.617	
		DevDist ↓	3.591	8.227	4.255	3.206	3.202	3.148	6.064	6.064	<u>3.064</u>	3.193	2.729
		TravelDist ↓	0.578	0.596	0.596	0.591	0.537	0.506	0.630	0.630	<u>0.436</u>	0.650	0.325
		DepartTime ↓	0.505	0.566	0.573	0.561	0.566	0.476	0.593	0.593	<u>0.297</u>	0.597	0.197
	Week	Acc ↑	0.463	0.469	0.518	0.561	0.561	0.539	0.523	0.523	<u>0.566</u>	0.521	0.612
		DevDist ↓	8.989	11.880	8.694	3.482	<u>3.224</u>	3.477	7.749	7.749	3.456	7.301	2.780
		TravelDist ↓	0.489	0.496	0.494	0.598	0.539	0.568	0.569	0.569	<u>0.484</u>	0.608	0.335
		DepartTime ↓	0.408	0.522	0.527	0.571	0.566	0.534	0.549	0.549	<u>0.383</u>	0.559	0.227
Tokyo	Day	Acc ↑	0.566	0.580	0.505	0.483	0.576	0.584	0.564	0.587	0.492	0.595	
		DevDist ↓	2.295	2.099	2.666	2.497	2.466	<u>2.010</u>	3.012	3.012	2.039	3.758	1.916
		TravelDist ↓	0.587	0.622	0.592	0.627	0.607	0.599	0.600	0.600	<u>0.567</u>	0.650	0.539
		DepartTime ↓	0.493	0.618	0.344	0.317	0.610	0.557	0.601	0.601	<u>0.275</u>	0.604	0.108
	Week	Acc ↑	0.472	0.568	0.504	0.457	0.565	<u>0.571</u>	0.559	0.559	<u>0.571</u>	0.486	0.588
		DevDist ↓	3.918	2.092	2.672	2.589	2.478	<u>2.051</u>	3.254	3.254	<u>2.450</u>	3.439	1.997
		TravelDist ↓	<u>0.549</u>	0.627	0.592	0.623	0.608	0.577	0.622	0.622	0.574	0.652	0.547
		DepartTime ↓	0.416	0.620	0.343	0.303	0.610	0.610	0.610	0.610	<u>0.297</u>	0.602	0.120

TABLE III
METRIC COMPARISON ON LA AND SFBay DATASETS.

			AGRAN	MTNet	HTAED	RLMob	MSTDP
LA	Day	Acc ↑	0.485	0.462	<u>0.550</u>	0.354	0.573
		DevDist ↓	4.982	5.005	4.194	6.412	3.818
		TravelDist ↓	0.648	0.684	<u>0.547</u>	0.686	0.422
		DepartTime ↓	0.661	0.667	<u>0.461</u>	0.674	0.374
	Week	Acc ↑	0.424	0.412	<u>0.445</u>	0.338	0.460
		DevDist ↓	5.304	5.492	<u>5.130</u>	6.542	4.921
		TravelDist ↓	0.656	0.674	<u>0.592</u>	0.685	0.477
		DepartTime ↓	0.673	0.673	<u>0.546</u>	0.677	0.392
SFBay	Day	Acc ↑	0.452	0.442	<u>0.529</u>	0.324	0.558
		DevDist ↓	6.818	7.210	<u>5.784</u>	10.576	5.222
		TravelDist ↓	0.645	0.670	<u>0.562</u>	0.679	0.436
		DepartTime ↓	0.587	0.666	<u>0.461</u>	0.673	0.372
	Week	Acc ↑	0.399	0.404	<u>0.416</u>	0.297	0.430
		DevDist ↓	7.660	7.883	<u>7.169</u>	10.706	6.945
		TravelDist ↓	0.664	0.672	<u>0.609</u>	0.684	0.493
		DepartTime ↓	0.598	0.675	<u>0.552</u>	0.680	0.384

primarily identify three patterns, with a notable emphasis on pattern ID=6, indicative of their focus on daily full-day stays. Our model adeptly captures these prevalent travel patterns, demonstrating performance superiority over HTAED through close alignment with the actual distribution.

Origin-Destination (OD) flow pairs. We collect the cell-level OD flow pairs between the actual and predicted flows and illustrate them in Figure 7. We calculate R^2 and CPC [52] between actual and predicted flows for numerical comparison. AGRAN and MTNet predict a limited number of flows, consistent with previous analyses indicating their preference for predicting full-day stays. HTAED overestimates flows with

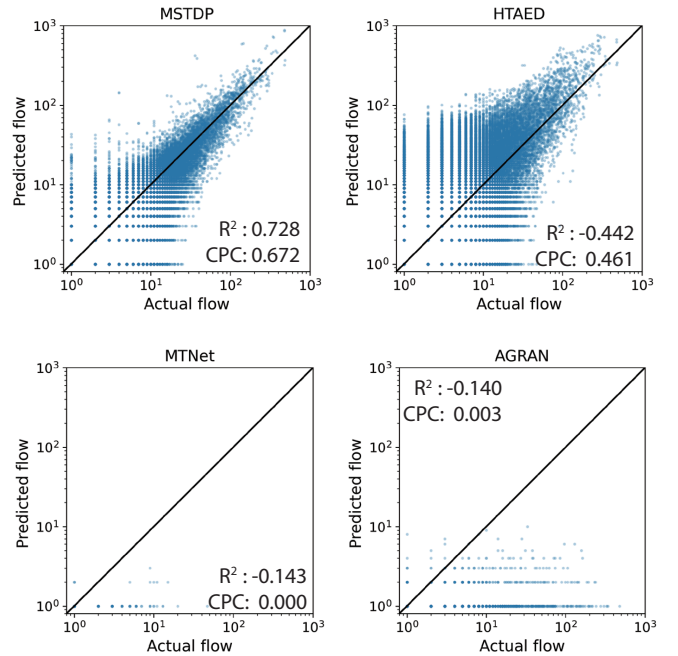


Fig. 7. Origin-Destination flow pairs between actual and predicted flows.

an R^2 of -0.442 and CPC of 0.461, whereas our MSTDP model achieves closer predictions to actual flow quantities, with an improved R^2 of 0.728 and CPC of 0.672.

Origin-Destination flows in map. Figure 8 illustrates the actual and predicted OD flows in the map, where the

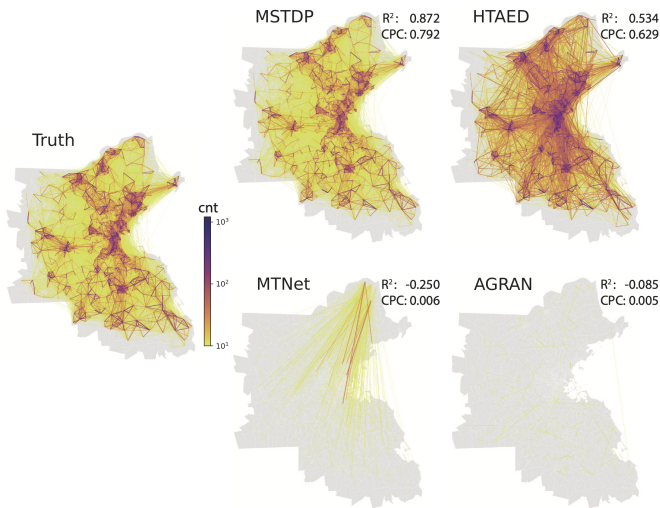


Fig. 8. Origin-Destination flows in tract level.

trips between cells are aggregated at the census tract level. The global travel patterns predicted by the three baseline models deviate significantly from the actual results. HTAED achieves R^2 and CPC values of 0.534 and 0.629, whereas MSTDP achieves 0.872 and 0.792, indicating performance improvements of 63.3% and 25.9% in our model. In this subsection, we examine OD flows at the cell and tract levels. Additionally, Figure 9 illustrates OD flows at the zip code level. MSTDP achieves R -squared (R^2) and CPC values of 0.969 and 0.877, while HTAED obtains 0.928 and 0.817. The performance improvements are 4.4% and 7.3%, respectively. This observation suggests that larger spatial aggregations may obscure differences between models.

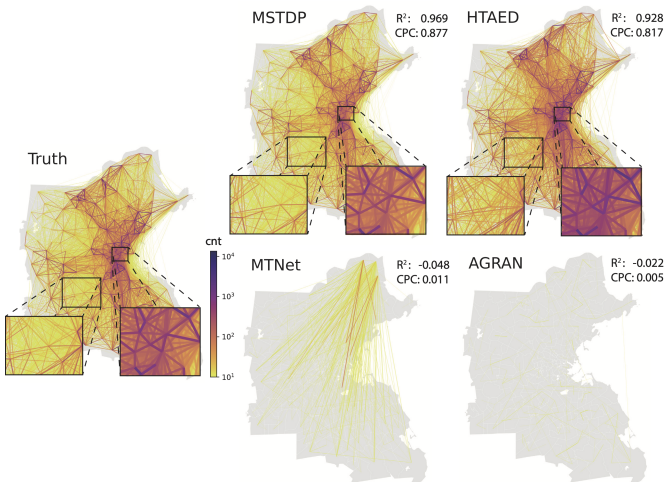


Fig. 9. Origin-Destination flows in zip code level.

Seven-day consecutive forecasting. We employ an iterative forecasting approach to predict future travel continuously throughout the upcoming week. The accuracy and deviation distance fluctuation of the predictions over seven days are illustrated in Figure 10. As the forecasting horizon extends, the accuracy of all models gradually diminishes, alongside

increased deviation distances between actual and predicted locations. This trend highlights the cumulative error inherent in iterative prediction approaches. Notably, when forecasting the subsequent second and third days, MSTDP exhibits slower performance degradation than HTAED. This disparity can be attributed to our model’s broader contextual awareness, leveraging 5 and 4 days of historical data for respective predictions.

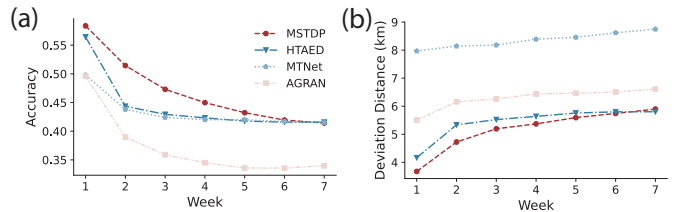


Fig. 10. Metrics of consecutive seven-day forecasts. (a) Accuracy; (b) Deviation distance.

D. Ablation Study

We compare MSTDP with three variants to examine the effectiveness of the modules in MSTDP. The ablated variants of MSTDP are as follows: (1) MSTDP-D: it eliminates the spatial-temporal decoupler and directly encodes the long trajectories; (2) MSTDP-H: it abandons the hierarchical structure and solely utilizes the daily encoder; (3) MSTDP-G: it replaces the graph-based location representation with a word embedder; (4) MSTDP-LD: the temporal decoder excludes the concatenation from location decoder and uses a Transformer decoder structure rather than the Transformer encoder.

The results in Table IV demonstrate that MSTDP outperforms these ablation variants, highlighting the effectiveness of each designed module. Among these variants, the MSTDP-H exhibits the weakest performance in both prediction tasks, likely due to reduced capability in capturing long-term dependencies and weekly periodicity following the removal of its hierarchical structure. MSTDP-LD exhibits inferior performance compared to MSTDP-D and MSTDP-G in next day prediction tasks, yet surpasses them in next week prediction tasks. This could be attributed to the incorporation of predicted locations in the temporal decoder, resulting in increased cumulative errors in next week predictions. Inaccuracies in location predictions adversely impact the model’s overall performance.

TABLE IV
ABLATION STUDIES ON *Boston* DATASET.

	Metrics	Acc \uparrow	DevDist \downarrow	TravelDist \downarrow	TravelTime \downarrow
Next Day Prediction	MSTDP-D	0.571	3.891	0.539	0.560
	MSTDP-H	0.448	5.003	0.426	0.450
	MSTDP-G	0.575	3.749	0.381	0.447
	MSTDP-LD	0.564	3.870	0.394	0.424
	MSTDP	0.584	3.676	0.361	0.419
Next Week Prediction	MSTDP-D	0.404	5.634	0.564	0.570
	MSTDP-H	0.383	5.747	0.472	0.464
	MSTDP-G	0.405	5.518	0.461	0.449
	MSTDP-LD	0.409	5.375	0.470	0.440
	MSTDP	0.413	5.369	0.455	0.438

E. Hyperparameter Analysis

To examine the MSTDP’s sensitivity to hyperparameters, we vary two hyperparameters to observe performance fluctuation. λ adjusts the weight of the temporal loss, impacting the optimization process. We test λ at values of 0.01, 0.1, 1, 10, and 100. Additionally, we also evaluate the head number (HN) of the attention in the Transformer encoder, considering values of 2, 4, and 8.

Table V presents the performance fluctuation with the hyperparameter variations. The results indicate that increasing the number of attention heads improves model performance. The influence of λ on performance fluctuations is relatively modest; larger values such as 1 or 100 yield superior results compared to smaller values like 0.1 or 0.01. This highlights the critical role of duration time learning.

TABLE V
HYPERPARAMETER ANALYSIS ON *Boston* DATASET.

		Acc \uparrow	DevDist \downarrow	TravelDist \downarrow	TravelTime \downarrow
Next Day Prediction	#Head = 2	0.568	3.826	0.392	0.426
	#Head = 4	0.571	3.803	0.389	0.430
	$\lambda = 0.01$	0.567	3.826	0.387	0.425
	$\lambda = 0.1$	0.569	3.825	0.395	0.430
	$\lambda = 10$	0.574	3.777	0.386	0.428
	$\lambda = 100$	0.571	3.786	0.400	0.421
	$\lambda = 1, \#Head = 8$	0.584	3.676	0.361	0.419
Next Week Prediction	#Head = 2	0.405	5.441	0.470	0.443
	#Head = 4	0.403	5.478	0.468	0.450
	$\lambda = 0.01$	0.404	5.470	0.467	0.445
	$\lambda = 0.1$	0.411	5.349	0.469	0.447
	$\lambda = 10$	0.407	5.445	0.465	0.444
	$\lambda = 100$	0.418	5.292	0.473	0.436
	$\lambda = 1, \#Head = 8$	0.413	5.369	0.455	0.438

F. Application to Epidemic Transmission

The predicted mid-term trajectory can be applied to urban management applications. To demonstrate its practicality, we use the example of epidemic transmission analysis. Urban areas are typically divided into multiple subspaces. Researchers employ epidemic transmission models to simulate the infection dynamics within each subspace. Meanwhile, individual trajectories are utilized to guide the movement of urban residents, reproducing the propagation of infection between different subspaces. Comparing the discrepancies in epidemic transmission dynamics between observed and predicted trajectories provides insights into the model’s predictive capacity for human mobility.

The SEIR model is commonly used to represent the epidemic spreading in a population [22], [53]. It categorizes all individuals into four states: susceptible (S), exposed (E), infectious (I), and removed (R). Susceptible individuals can become infected through close contact with those carrying the infection and subsequently transition into the exposed state. There exists a probability of transitioning from the exposed state to infection. Lastly, infectious individuals transition into the removed state with a probability. The removed state assumes that individuals are no longer infected and cannot transmit the infection to others. Specifically, the probability of being exposed is formulated as $P_{\text{exp},i} = \frac{\alpha\beta I_i}{N_i}$, where α is the number of close contacts, β is the infectious rate, I_i and N_i stand for

the number of infectious people and total population in the i -th subregion of the city. The infectious probability P_{inf} is the inverse of the average incubation period, while the removed probability P_{rem} is the inverse of the infectious period. The detailed parameter settings are illustrated in Table VI. R_0 , the basic reproduction number, represents the average number of secondary infections caused by an infectious individual. It is calculated as the product of α, β , and the average infectious period.

TABLE VI
PARAMETER SETTINGS IN SEIR MODEL.

Parameter	Value	Parameter	Value
α	0.4	β	0.1
Incubation Period	3*24	P_{inf}	$\frac{1}{3 \times 24}$
Infection Period	7*24	P_{rem}	$\frac{1}{7 \times 24}$
R_0	6.72		

In this study, due to the sparse population in the dataset, we initially aggregate cell-level trajectories to the admin level (census tract for *Boston*) and assign an SEIR epidemic model to each administrative area. Subsequently, we employ these trajectories to construct a population transition probability matrix for each time window. These matrices are normalized to represent the probability of individuals choosing to stay or move between administrative areas during different periods. The population of each administrative area is obtained from Worldpop². For each time window, we first employ the SEIR model to calculate the status change of individuals within each administrative area, and then determine individual movement based on the transition probability matrix. All individuals are considered independent of each other.

We conduct 100 independent experiments using the actual data on *Boston* dataset and the trajectories from seven-day consecutive forecasting with models. In each experiment, we randomly initialize 1000 infected individuals and monitor the half-hour fluctuations in the current active cases (I) and cumulative new cases ($\sum \Delta$) throughout the week. These predictive models are evaluated by comparing the infection numbers derived from the real and the predicted trajectories. The top-performing baseline, HTAED, is selected for comparison. We apply Mean Absolute Error (MAE) as the evaluation metric, and the average MAE is shown in Figure 11.

The experimental results indicate that the MAE of all models is comparatively low in the initial three days due to the setting of a three-day incubation period. However, beyond the fourth day, the MAE curve of the baseline model exhibits increasing divergence, while the MSTDP model consistently maintains a lower MAE. This difference can be attributed to the enhanced predictive capabilities of the MSTDP model in comparison to the baseline model in forecasting travel patterns. We calculate the half-hour average MAE for the seventh day for numerical comparison. The MAE (I) values for MSTDP and HTAED are 17.1 and 138.5, while the MAE ($\sum \Delta$) values are 96.2 and 258.8. The performance improvement of MSTDP

²<https://www.worldpop.org/>

is 87.6% and 62.8%, respectively. HTAED incurs a larger MAE due to its prediction of increased travel behaviors, which accelerates virus transmission and consequently leads to higher infection rates.

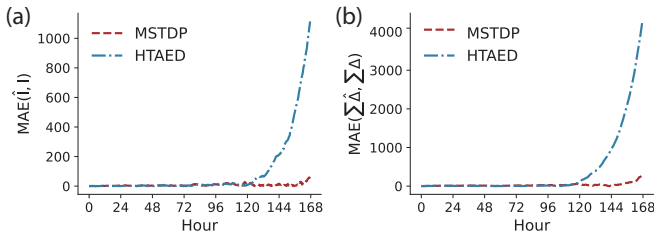


Fig. 11. MAE over time. (a) The current active cases (I); (b) The cumulative new cases ($\sum \Delta$).

VI. CONCLUSION

This study addresses mid-term human mobility prediction, a crucial task for understanding the daily travel patterns among urban residents and advancing urban science applications. We propose a novel approach, Multi-Scale Spatial-Temporal Decoupled Predictor (MSTDP), which employs a spatial-temporal decoupler and a hierarchical encoder to capture transition patterns across multiple time scales. Furthermore, we introduce a spatial heterogeneous graph to effectively represent the flow and spatial relationships between locations, facilitating the learning of semantic-rich location representation. We conduct extensive experiments to analyze the model's performance and demonstrate its effectiveness. Specifically, we evaluate MSTDP against nine baselines using five urban-scale mobile record datasets, demonstrating its superior performance. The statistical analysis, using Boston as a case study, examines key factors such as travel motifs, distances, and origin-destination flows in predicted trajectories. The results highlight that existing baseline models fail to accurately replicate the macro-level statistical patterns of individual mobility, whereas our proposed model effectively captures these patterns, underscoring its superior capability in modeling urban travel dynamics. Additionally, we apply the predictions to simulate epidemic dynamics with the SEIR model, using population transfer matrices derived from travel trajectories. The results show substantial improvements over the baselines, with reductions in MAE of 87.6% for cumulative new cases and 62.8% for active cases, highlighting MSTDP's superior predictive capabilities in mobility modeling.

REFERENCES

- [1] R. Wu, G. Luo, J. Shao, L. Tian, and C. Peng, "Location prediction on trajectory data: A review," *Big data mining and analytics*, 2018.
- [2] Y. Xu, S. Çolak, E. C. Kara, S. J. Moura, and M. C. González, "Planning for electric vehicle needs by coupling charging profiles with urban mobility," *Nature Energy*, vol. 3, no. 6, pp. 484–493, 2018.
- [3] Z. Zhou, K. Yang, Y. Liang, B. Wang, H. Chen, and Y. Wang, "Predicting collective human mobility via countering spatiotemporal heterogeneity," *IEEE Transactions on Mobile Computing*, 2023.
- [4] W. Jia, S. Zhao, and K. Zhao, "Human mobility prediction based on trend iteration of spectral clustering," *IEEE Transactions on Mobile Computing*, vol. 23, no. 5, pp. 4196–4211, 2023.
- [5] S. Xu, X. Fu, J. Cao, B. Liu, and Z. Wang, "Survey on user location prediction based on geo-social networking data," *WWW*, 2020.
- [6] J. S. Jia, X. Lu, Y. Yuan, G. Xu, J. Jia, and N. A. Christakis, "Population flow drives spatio-temporal distribution of covid-19 in china," *Nature*, vol. 582, no. 7812, pp. 389–394, 2020.
- [7] M. Luca, B. Lepri, E. Frias-Martinez, and A. Lutu, "Modeling international mobility using roaming cell phone traces during covid-19 pandemic," *EPJ Data Science*, vol. 11, no. 1, p. 22, 2022.
- [8] Y. Xu, L. E. Olmos, D. Mateo, A. Hernando, X. Yang, and M. C. González, "Urban dynamics through the lens of human mobility," *Nature Computational Science*, vol. 3, no. 7, pp. 611–620, 2023. [Online]. Available: <https://doi.org/10.1038/s43588-023-00484-5>
- [9] C. Chen, D. Zhang, N. Li, and Z.-H. Zhou, "B-planner: Planning bidirectional night bus routes using large-scale taxi gps traces," *IEEE TITS*, 2014.
- [10] Y. Xu, R. D. Clemente, and M. C. González, "Understanding vehicular routing behavior with location-based service data," *EPJ Data Science*, vol. 10, no. 1, pp. 1–17, 2021.
- [11] J. Ji, J. Wang, C. Huang, J. Wu, B. Xu, Z. Wu, J. Zhang, and Y. Zheng, "Spatio-temporal self-supervised learning for traffic flow prediction," *arXiv preprint arXiv:2212.04475*, 2022.
- [12] M. Luca, G. Barlacchi, B. Lepri, and L. Pappalardo, "A survey on deep learning for human mobility," *ACM Computing Surveys (CSUR)*, 2021.
- [13] S. Feng, X. Li, Y. Zeng, G. Cong, and Y. M. Chee, "Personalized ranking metric embedding for next new poi recommendation," in *IJCAI*, 2015.
- [14] Q. Guo, Z. Sun, J. Zhang, and Y.-L. Theng, "An attentional recurrent neural network for personalized next location recommendation," in *AAAI*, 2020.
- [15] L. Zhang, Z. Sun, Z. Wu, J. Zhang, Y. S. Ong, and X. Qu, "Next point-of-interest recommendation with inferring multi-step future preferences," in *IJCAI*, 2022.
- [16] S. Yang, J. Liu, and K. Zhao, "Getnext: trajectory flow map enhanced transformer for next poi recommendation," in *SIGIR*, 2022.
- [17] Z. Wang, Y. Zhu, H. Liu, and C. Wang, "Learning graph-based disentangled representations for next poi recommendation," in *SIGIR*, 2022.
- [18] N. Lim, B. Hooi, S.-K. Ng, Y. L. Goh, R. Weng, and R. Tan, "Hierarchical multi-task graph recurrent network for next poi recommendation," in *SIGIR*, 2022.
- [19] Y. Qin, Y. Wang, F. Sun, W. Ju, X. Hou, Z. Wang, J. Cheng, J. Lei, and M. Zhang, "Disenpoi: Disentangling sequential and geographical influence for point-of-interest recommendation," in *WDSM*, 2023.
- [20] X. Yan, T. Song, Y. Jiao, J. He, J. Wang, R. Li, and W. Chu, "Spatio-temporal hypergraph learning for next poi recommendation," in *Proceedings of the 46th International ACM SIGIR Conference on Research and Development in Information Retrieval*, 2023, pp. 403–412.
- [21] G. Jin, Y. Liang, Y. Fang, Z. Shao, J. Huang, J. Zhang, and Y. Zheng, "Spatio-temporal graph neural networks for predictive learning in urban computing: A survey," *IEEE Transactions on Knowledge and Data Engineering*, 2023.
- [22] S. Chang, E. Pierson, P. W. Koh, J. Gerardin, B. Redbird, D. Grusky, and J. Leskovec, "Mobility network models of covid-19 explain inequities and inform reopening," *Nature*, vol. 589, no. 7840, pp. 82–87, 2021.
- [23] C. Cheng, H. Yang, M. R. Lyu, and I. King, "Where you like to go next: Successive point-of-interest recommendation," in *IJCAI*, 2013.
- [24] S. Jiang, Y. Yang, S. Gupta, D. Veneziano, S. Athavale, and M. C. González, "The timegeo modeling framework for urban mobility without travel surveys," *Proceedings of the National Academy of Sciences*, vol. 113, no. 37, pp. E5370–E5378, 2016.
- [25] J. Feng, Y. Li, C. Zhang, F. Sun, F. Meng, A. Guo, and D. Jin, "Deep-move: Predicting human mobility with attentional recurrent networks," in *WWW*, 2018.
- [26] Y. Xu, J. Xu, J. Zhao, K. Zheng, A. Liu, L. Zhao, and X. Zhou, "Metaptp: An adaptive meta-optimized model for personalized spatial trajectory prediction," in *KDD*, 2022.
- [27] K. Sun, T. Qian, T. Chen, Y. Liang, Q. V. H. Nguyen, and H. Yin, "Where to go next: Modeling long-and short-term user preferences for point-of-interest recommendation," in *AAAI*, 2020.
- [28] Y. Luo, Q. Liu, and Z. Liu, "Stan: Spatio-temporal attention network for next location recommendation," in *WWW*, 2021.
- [29] D. Lian, Y. Wu, Y. Ge, X. Xie, and E. Chen, "Geography-aware sequential location recommendation," in *KDD*, 2020.
- [30] Y. Lin, H. Wan, S. Guo, and Y. Lin, "Pre-training context and time aware location embeddings from spatial-temporal trajectories for user next location prediction," in *AAAI*, 2021.

- [31] X. Wang, G. Sun, X. Fang, J. Yang, and S. Wang, "Modeling spatio-temporal neighbourhood for personalized point-of-interest recommendation," in *IJCAI*, 2022.
- [32] Y. Qin, C. Gao, Y. Wang, S. Wei, D. Jin, J. Yuan, and L. Zhang, "Disentangling geographical effect for point-of-interest recommendation," *IEEE Transactions on Knowledge and Data Engineering*, 2022.
- [33] T. Huang, X. Pan, X. Cai, Y. Zhang, and X. Yuan, "Learning time slot preferences via mobility tree for next poi recommendation," in *Proceedings of the AAAI Conference on Artificial Intelligence*, vol. 38, no. 8, 2024, pp. 8535–8543.
- [34] N. Jiang, H. Yuan, J. Si, M. Chen, and S. Wang, "Towards effective next poi prediction: Spatial and semantic augmentation with remote sensing data," *arXiv preprint arXiv:2404.04271*, 2024.
- [35] F. Yu, L. Cui, W. Guo, X. Lu, Q. Li, and H. Lu, "A category-aware deep model for successive poi recommendation on sparse check-in data," in *WWW*, 2020.
- [36] Z. Dong, X. Meng, and Y. Zhang, "Exploiting category-level multiple characteristics for poi recommendation," *IEEE Transactions on Knowledge and Data Engineering*, 2021.
- [37] Z. Huang, S. Xu, M. Wang, H. Wu, Y. Xu, and Y. Jin, "Human mobility prediction with causal and spatial-constrained multi-task network," *EPJ Data Science*, vol. 13, no. 1, p. 22, 2024.
- [38] F. Li, Z. Gui, Z. Zhang, D. Peng, S. Tian, K. Yuan, Y. Sun, H. Wu, J. Gong, and Y. Lei, "A hierarchical temporal attention-based lstm encoder-decoder model for individual mobility prediction," *Neurocomputing*, vol. 403, pp. 153–166, 2020.
- [39] Z. Luo and C. Miao, "Rlmob: Deep reinforcement learning for successive mobility prediction," in *Proceedings of the Fifteenth ACM International Conference on Web Search and Data Mining*, 2022, pp. 648–656.
- [40] H. Han, M. Zhang, M. Hou, F. Zhang, Z. Wang, E. Chen, H. Wang, J. Ma, and Q. Liu, "Stgcn: a spatial-temporal aware graph learning method for poi recommendation," in *ICDM*, 2020.
- [41] F. Yin, Y. Liu, Z. Shen, L. Chen, S. Shang, and P. Han, "Next poi recommendation with dynamic graph and explicit dependency," in *Proceedings of the AAAI Conference on Artificial Intelligence*, vol. 37, no. 4, 2023, pp. 4827–4834.
- [42] Z. Wang, Y. Zhu, C. Wang, W. Ma, B. Li, and J. Yu, "Adaptive graph representation learning for next poi recommendation," in *Proceedings of the 46th International ACM SIGIR Conference on Research and Development in Information Retrieval*, 2023, pp. 393–402.
- [43] X. Wang, F. Fukumoto, J. Cui, Y. Suzuki, J. Li, and D. Yu, "Eedn: Enhanced encoder-decoder network with local and global context learning for poi recommendation," in *Proceedings of the 46th International ACM SIGIR Conference on Research and Development in Information Retrieval*, 2023, pp. 383–392.
- [44] Z. Wang, Y. Zhu, Q. Zhang, H. Liu, C. Wang, and T. Liu, "Graph-enhanced spatial-temporal network for next poi recommendation," *TKDD*, 2022.
- [45] C. M. Schneider, V. Belik, T. Couronné, Z. Smoreda, and M. C. González, "Unravelling daily human mobility motifs," *Journal of The Royal Society Interface*, 2013.
- [46] W. Hamilton, Z. Ying, and J. Leskovec, "Inductive representation learning on large graphs," *NeurIPS*, 2017.
- [47] P. Velickovic, G. Cucurull, A. Casanova, A. Romero, P. Lio, Y. Bengio *et al.*, "Graph attention networks," *ICLR*, 2017.
- [48] A. Vaswani, N. Shazeer, N. Parmar, J. Uszkoreit, L. Jones, A. N. Gomez, E. Kaiser, and I. Polosukhin, "Attention is all you need," *NeurIPS*, 2017.
- [49] T. Yabe, K. Tsubouchi, T. Shimizu, Y. Sekimoto, K. Sezaki, E. Moro, and A. Pentland, "Metropolitan scale and longitudinal dataset of anonymized human mobility trajectories," *arXiv preprint arXiv:2307.03401*, 2023.
- [50] X. Rao, L. Chen, Y. Liu, S. Shang, B. Yao, and P. Han, "Graph-flashback network for next location recommendation," in *KDD*, 2022.
- [51] Y. Tang, J. He, and Z. Zhao, "Hgarn: Hierarchical graph attention recurrent network for human mobility prediction," *arXiv preprint arXiv:2210.07765*, 2022.
- [52] M. Lenormand, A. Bassolas, and J. J. Ramasco, "Systematic comparison of trip distribution laws and models," *Journal of Transport Geography*, vol. 51, pp. 158–169, 2016.
- [53] S. Lai, N. W. Ruktanonchai, L. Zhou, O. Prosper, W. Luo, J. R. Floyd, A. Wesolowski, M. Santillana, C. Zhang, X. Du *et al.*, "Effect of non-pharmaceutical interventions to contain covid-19 in china," *nature*, vol. 585, no. 7825, pp. 410–413, 2020.